View metadata, citation and similar papers at core.ac.uk
brought to you by CORE
provided by Open Access LMU

Reorientational Dynamics and Solid-Phase Transformation of Ammonium Dicyanamide into Dicyandiamide: A ^{2}H Solid-State NMR Study

Bettina V. Lotsch,[†,||] Wolfgang Schnick,[†] Ernst Naumann,[‡] and Jürgen Senker*[,§]

Department Chemie und Biochemie, Ludwig-Maximilians-Universität, Butenandtstrasse 5-13 (D), 81377 München, Germany, Bruker Elektronik GmbH, Silberstreifen 29, 76287 Rheinstetten, Germany, and Anorganische Chemie I, Universität Bayreuth, Universitätsstrasse 30, 95447 Bayreuth, Germany

Received: March 6, 2007; In Final Form: July 15, 2007

The reorientational dynamics of ammonium dicyanamide $ND_4[N(C{\equiv}N)_2]$ and the kinetics as well as the mechanism of the solid-state isomerization reaction from ammonium dicyanamide into dicyandiamide ($N{\equiv}C{-}N{=}C(NH_2)_2$) was studied by means of ^{2}H and ^{14}N solid-state NMR spectroscopy in a temperature range between 38 and 390 K. Whereas in previous investigations the mechanism of the solid-state transformation was investigated by means of vibrational and magic angle spinning solid-state NMR spectroscopy as well as neutron diffraction, we here present a comprehensive ^{2}H study of the ammonium ion dynamics prior to and during the course of the reaction, thereby highlighting possible cross correlations between dynamics and reactivity involving the ammonium ion. The ND_4^+ group was found to undergo thermally activated random jumps in a tetrahedral potential, which is increasingly distorted with increasing temperature, giving rise to an asymmetrically compressed or elongated tetrahedron with deviations from the tetrahedral angle of up to 6°. The correlation time follows an Arrhenius law with an activation energy of $E_a = 25.8(2)$ kJ mol^{-1} and an attempt frequency of $\tau_0^{-1} = 440(80)$ THz. The spin−lattice relaxation times were fitted according to a simple Bloembergen−Purcell−Pound type model with a T_1 minimum of 4 ms at 230 K. Temperature-dependent librational amplitudes were extracted by line-shape simulations between 38 and 390 K and contrasted with those obtained by neutron diffraction, their values ranging between 5 and 28°. The onset and progress of the solid-phase transformation were followed in situ at temperatures above 372 K and could be classified as a strongly temperature-dependent, heterogeneous two-step reaction proceeding with rapid evolution of ammonia and comparatively slow subsequent reintegration into the solid. On the microscopic level, this correlates with a rapid proton transfer—possibly triggered by a coupling between the ammonium ion dynamics and phonon modes on the terahertz time scale—and an essentially decoupled nucleophilic attack of ammonia at the nitrile carbon, giving rise to significantly differing time constants for the two processes.

Introduction

Ammonium dicyanamide $NH_4[N(C{\equiv}N)_2]$ (NH_4dca) was investigated in some detail recently owing to its intriguing solid-phase reactivity, which was evaluated on the background of constructing condensed CN_x materials for the synthesis of graphitic carbon nitride g-C_3N_4.[1−15] NH_4dca may be considered an isolobal analogue of Wöhler's historically important compound ammonium cyanate $NH_4[OCN]$, which had given birth to a new conceptual approach to modern chemistry.[16−18] At temperatures beyond 353 K, ammonium dicyanamide transforms into its molecular isomer dicyandiamide ($N{\equiv}C{-}N{=}C(NH_2)_2$) in a topochemical reaction without passing through the melt, which can be viewed in direct analogy with the conversion of ammonium cyanate into urea $O{=}C(NH_2)_2$.[19−22] Above 440 K, dicyandiamide is converted into melamine, $C_3N_3(NH_2)_3$, which then polymerizes forming highly condensed CN_xH_y species such as melon.[5,12,14,15] Owing to the above facile transformations, ammonium dicyanamide has entered the focus as a suitable model system for the study of solid-state reactivity in molecular systems, which despite its relevance with respect to both fundamental and explorative solid-state chemistry has until recently been largely neglected. Previously, we investigated structural aspects as well as the thermal conversion of NH_4dca by a broad spectrum of analytical techniques, such as in situ single-crystal X-ray and neutron powder diffraction, ^{15}N and ^{13}C solid-state NMR spectroscopy, vibrational spectroscopy, and thermal analysis.[21,22] Those studies indicated that the time frame of the conversion of NH_4dca into dicyandiamide might well be influenced by the reorientational dynamics of the ammonium ions, which shall therefore be addressed in the present work.

When the time average of the nuclear density is traced, neutron diffraction allows for the determination of the probability density function (*pdf*), therefore providing the a priori probabilities for the site occupation of the four deuteron nuclei of the ammonium group.[23,24] On the other hand, solid-state NMR—by offering an intriguing single-particle perspective owing to the dominant effect of the local quadrupolar interaction on the spectra—is a valuable resource for gaining insight into *dynamical* processes in solid materials on a large time scale. The study of fast motions ($\tau^{-1} = 10^8{-}10^{12}$ Hz) can be addressed by spin−lattice relaxation, whereas for intermediate time scales ($10^3{-}10^8$ Hz), line-shape simulations of one-dimensional quadrupolar spectra have proven to be exceptionally

* To whom correspondence should be addressed. E-mail: juergen.senker@uni-bayreuth.de.
[†] Ludwig-Maximilians-Universität.
[‡] Bruker Elektronik GmbH.
[§] Universität Bayreuth.
[||] Current address: Lash Miller Chemical Laboratory, Department of Chemistry, University of Toronto, 80 St. George Street, M5S 3H6, Canada.

10.1021/jp071823e CCC: $37.00 © 2007 American Chemical Society
Published on Web 09/19/2007

SCHEME 1: Two Possible Reaction Pathways for the Solid-State Isomerization of Ammonium Dicyanamide into Dicyandiamide[a]

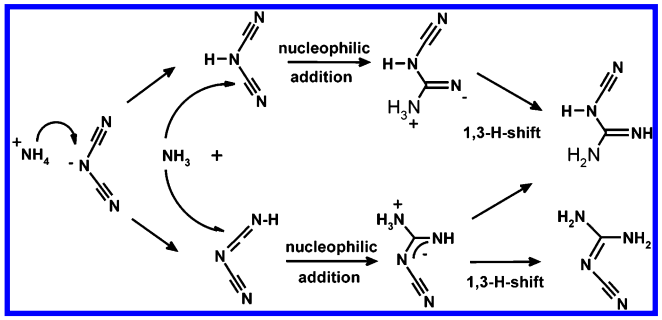

[a] Top: proton transfer from the ammonium ion to the central amido-nitrogen of the anion. Bottom: protonation at one of the nitrile nitrogen atoms.

versatile tools for extracting detailed models of motion for the reorienting species involved. Processes in the slow motion limit ($\tau^{-1} = 10^{-2}-10^{4}$ Hz) can be probed by exchange spectra and stimulated echo techniques.[25−28] Traditionally, ^{2}H NMR spectroscopy is used as a powerful technique for the study of dynamics in glassy systems, liquid crystals, and polymers, with the emphasis being on structural phase and glass transitions of essentially amorphous systems.[25,26,29−35] In addition, ^{2}H NMR in conjunction with neutron scattering afforded a better understanding of the cross-link between structural and dynamic phenomena and provided new insights into relaxation and tunneling processes[36−39] in simple crystalline salts, among which ammonium compounds such as NH_4Cl[40−43] or $(NH_4)_2SO_4$ play a prominent role. Accordingly, applying the ^{2}H NMR technique to the in situ study of the topochemical transformation of ammonium dicyanamide into dicyandiamide seems to be a straightforward issue, which will be discussed in some detail in the present work. As a guiding theme, the impact of ammonium ion reorientation on the solid-phase transformation shall be assessed by elaborating the ammonium ion dynamics throughout the pretransformation regime, followed by the in situ monitoring of the ammonium ion reactivity during the transformation. By taking into account symmetry restrictions imposed by the deuteron *pdf* into the analysis of the ^{2}H NMR data, we are capable of correlating structural and dynamic information and, thus, may enter the realm of solid-state reactivity.

Properties of Ammonium Dicyanamide. The solid-state transformation of ammonium dicyanamide into dicyandiamide was classified as a *topochemical* solid-state reaction proceeding in a *nontopotactic* fashion, yet with minimal molecular movement and structural changes under carefully controlled temperature conditions.[21,22] Temperature-programmed Raman and ^{15}N as well as ^{13}C solid-state NMR spectroscopy allowed us to draw a comprehensive picture of the transformation mechanism, which can be described as an initial proton transfer from the ammonium ion to one of the terminal nitrogen atoms of the nitrile groups, followed by a nucleophilic addition of the as-formed ammonia to the adjacent electrophilic carbon (Scheme 1).[22] Furthermore, these data indicate that the ammonium ions perform relaxational large angle jumps.[22]

Neutron diffraction studies gave evidence of a pronounced additional anisotropic librational mobility of the ND_4^+ group with rising temperature (Figure 1), along with significant distortion of the hydrogen-bonding network, including major *asymmetric* differences in the D−N−D bond angles and the N−D distances.[21] Correlated with the increasing distortion of

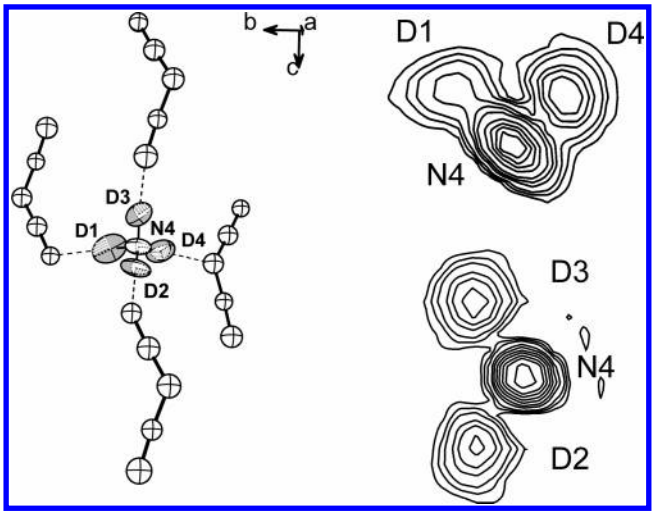

Figure 1. Representation of the deuteron nuclear density in $ND_4[N(C{\equiv}N)_2]$ as obtained by neutron diffraction. Left: Atom labeling scheme, shown for the cation−anion coordination sphere in $ND_4[N(C{\equiv}N)_2]$ at 295 K ($P2_1/c$, $a = 3.7913(8)$ Å, $b = 12.412(2)$ Å, $c = 9.113(2)$ Å). Right: Fourier maps representing the nuclear probability density function (*pdf*) of D1/D4 (*a*/*b*-plane, top) and D2/D3 (*a*/*c*-plane, bottom) at 365 K, map size 360 × 360 pm. Data taken from refs 21 and 22.

the ammonium ions toward higher temperatures is the contraction of the crystallographic *c*-axis, whereas the *a*- and *b*-axes elongate. Presumably the same lattice modes responsible for the unusual temperature dependence of the *c*-axis also cause the distortion of the ammonium ions from ideal tetrahedral symmetry.

Within the perspective of these observations our general strategy for the interpretation of the here presented ^{2}H NMR data shall be discussed briefly. The crystallographically observed distortion of the ammonium ions from ideal tetrahedral symmetry suggest nonzero averaged quadrupole-coupling tensors even in the limit of fast motion ($\tau < 10^{-6}$ s). As a consequence, narrow but non-Lorentzian line shapes are expected in this regime, which indeed are observed (Figure 2, middle). However, as pointed out in the literature,[36−43] external factors, such as electric field gradient asymmetries due to the surrounding of the ammonium group, may give rise to similar spectral features, thereby yielding a complex interplay between external and internal contributions to the electric field gradient (EFG).

To separate internal and external contributions to the EFG and to quantify the influence of either process on the ^{2}H line shapes, extensive quantum chemical calculations will be needed, which are beyond the scope of this paper. As a tendency, external electric field gradients are expected to dominate systems with rather shallow potentials and consequently low rotational activation barriers, whereas for deep energy wells internal distortions increasingly take effect on the NMR line shapes.

As the rotational activation energy obtained for the ammonium group in ND_4dca is one of the largest observed for ND_4^+ ions (see below), and since the distortion of the tetrahedral symmetry was independently proven by neutron powder diffraction, we will focus exclusively on the internal contribution to the EFG for the simulation of the ^{2}H line shapes. Thus, the resulting distortions of the ND_4^+ ions have to be understood as an upper limit when external contributions to the EFG are neglected.

Theoretical Basis

In the following we will only give a short account of the theoretical background by reviewing the essentials of ^{2}H line-

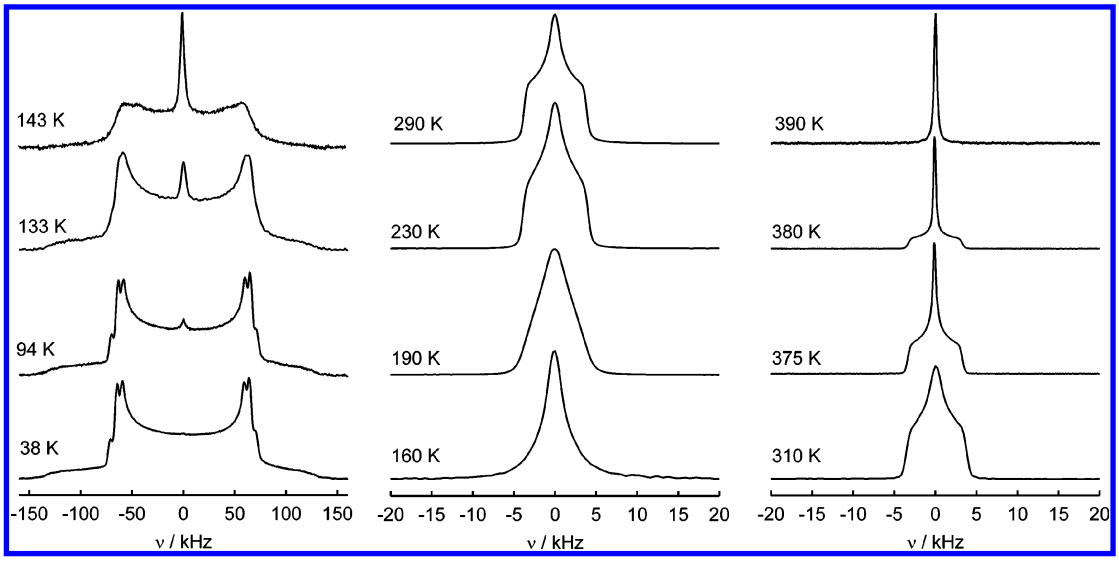

Figure 2. Representative solid−echo ^{2}H spectra of $ND_4[N(C{\equiv}N)_2]$ as a function of temperature between 38 and 390 K.

shape analysis. For a more detailed treatment of the topic see refs 25, 26, and 44−49.

Line-Shape Analysis. The physical phenomenon exploited by ^{2}H NMR spectroscopy is the interaction of the quadrupole moment of the deuteron spin with the electric field gradient (EFG) tensor present at the atomic site. For a covalently bonded deuterium atom the EFG is completely dominated by the electron distribution in the σ-bond and can therefore be treated as axially symmetric in good approximation. The principal axis system (PAS) can be correlated with an orthonormal molecular frame, the so-called crystal axis system (CAS), which is defined with respect to the symmetry of the molecule and its reorientational dynamics. The resonance frequency ω is thus a function of the orientation of the PAS of the EFG with respect to the laboratory axis system (LAS) determined by the external magnetic field.

In the presence of motion, the quadrupole-coupling tensor of a single deuteron can switch between i different sites, whose orientations are defined with respect to the CAS for convenience. The site frequencies may be calculated taking into account only the secular part of the quadrupolar Hamiltonian using irreducible second rank tensor operators.

$$\omega = \pm\sqrt{\frac{3}{2}}\frac{e^2qQ}{2\hbar}\sum_{n,a=-2}^{2}\rho_{2n}D_{na}^{(2)}(\Omega^{PC})D_{a0}^{(2)}(\Omega^{CL}) \quad (1)$$

The Eulerian transformations $\Omega = (\alpha,\beta,\gamma)$ represent the Wigner rotation matrices rotating the PAS into the CAS (Ω^{PC}) and the CAS into the LAS (Ω^{CL}) according to the convention by Rose as delineated by Spiess.[50] In the PAS, the only nonvanishing elements of the quadrupole-coupling tensor ρ are $\rho_{20} = (3/2)^{1/2}$ and $\rho_{2\pm2} = {}^1/_2\eta$ with η being the asymmetry parameter ($0 \le \eta \le 1$). The latter is defined by the Cartesian components of the coupling tensor according to $\eta = (\rho_{XX}^{(2)} - \rho_{YY}^{(2)}/\rho_{ZZ}^{(2)})$ with $|\rho_{ZZ}^{(2)}| \ge |\rho_{YY}^{(2)}| \ge |\rho_{XX}^{(2)}|$.

The reorientational dynamics can be treated according to a stationary Markov process, where the time-dependent change of the FID G(t) can be described by a Bloch−McConnel type equation

$$\frac{d\bar{G}}{dt} = \bar{G}(i\omega + \pi) \quad (2)$$

The elements of the row vector $\bar{G}$ are the complex transverse magnetization vectors associated with one component of the quadrupolar doublet arising from each of the orientational sites in a static scenario. ω is a diagonal matrix ($\omega_{ij} = \delta_{ij}\omega_j\Omega_j$) representing the site frequencies associated with the jumping site Ω_j, and π denotes the exchange matrix containing the jump frequencies π_{ij}. For reasons of microreversibility, the elements π_{ij} must fulfill the "detailed-balance" condition

$$p_i\pi_{ij} = p_j\pi_{ij} \quad (3)$$

where p_j is the a priori probability of finding the deuteron on site j and π is a symmetric matrix only if all a priori probabilities are equal. The diagonal elements are always the negative sum over a column, thus $\sum_i\pi_{ij} = 0$.

For the ammonium ion in $NH_4[N(C{\equiv}N)_2]$, 180° and 120° jumps about one single C_2 or C_3 axis of the tetrahedron, respectively, were considered, as well as isotropic four-site exchange in a 4-fold potential. The exchange matrices for the different processes are given by eqs 4−6.

$$\begin{pmatrix} -1 & 1 & 0 & 0 \\ 1 & -1 & 0 & 0 \\ 0 & 0 & -1 & 1 \\ 0 & 0 & 1 & -1 \end{pmatrix} \quad (4)$$

$$\begin{pmatrix} 0 & 0 & 0 & 0 \\ 0 & -2 & 1 & 1 \\ 0 & 1 & -2 & 1 \\ 0 & 1 & 1 & -2 \end{pmatrix} \quad (5)$$

$$\begin{pmatrix} -3 & 1 & 1 & 1 \\ 1 & -3 & 1 & 1 \\ 1 & 1 & -3 & 1 \\ 1 & 1 & 1 & -3 \end{pmatrix} \quad (6)$$

Apart from checking scenarios with the above idealized exchange mechanisms, various intermediate scenarios were also taken into account by systematically grading the exchange frequencies for particular sites. Thus, a four-site exchange process can be gradually assimilated to a three-site exchange by decreasing the exchange frequencies for one particular site i, with eq 3 still being valid.

The jump rates π_{ij} can be extracted from solid−echo spectra, whose line shapes can be calculated as the Fourier transform of the echo decay

$$K(t,t_1) = \bar{1} \exp((-i\omega + \pi)(t - t_1)) \exp((i\omega + \pi)t_1)\, \bar{G}(0) \quad (7)$$

where $t > t_1$ (t_1, interpulse distance) and the column vector $\bar{G}(0)$ represents the a priori probabilities p_j.

Spin−Lattice Relaxation. The spin−lattice relaxation rate is determined by the transitions among the Zeeman levels, i.e., the eigenstates of the Zeeman Hamiltonian. To obtain correlation times on a larger time scale than accessible by line-shape analysis, the spin−lattice relaxation constant T_{1Z}^{-1} for isotropic reorientation is determined via the spectral density J at the Larmor frequency ω_0:[44]

$$\frac{1}{T_{1Z}} = \frac{3}{40}\,\mathrm{QCC}^2\,[J(\omega_0) + 4J(2\omega_0)] \quad (8)$$

where QCC (QCC $= e^2Qq\hbar^{-1}$ and QCC/$2\pi = e^2Qqh^{-1}$) is the quadrupole-coupling constant.

The above so-called Bloembergen−Purcell−Pound (BPP) spectral density approach is only valid for stochastic Markovian processes with a unique correlation time and overall isotropic motion (cf. eq 2). From the spectral density at the Larmor frequency ω_0

$$J(\omega_0) = \frac{\tau}{1 + {\omega_0}^2\tau^2} \quad (9)$$

we can extract the correlation times τ and, by assuming Arrhenius-type behavior, the energy of activation $E_a(T)$ as well as the attempt frequency ${\tau_0}^{-1}$

$$\tau = \tau_0 \exp\left(\frac{E_a}{RT}\right) \quad (10)$$

Experimental Methods

Ammonium dicyanamide was prepared and deuterated according to a procedure described in ref 22. Static powder spectra were obtained on a DSX Avance 500 solid-state NMR spectrometer (Bruker, Karlsruhe) at a resonance frequency of 76.91 MHz (^{2}H) between 38 and 390 K or 36.149 MHz (^{14}N) at 160 and 293 K. Typically the finely powdered sample (150 mg) was filled into ultraprecision NMR glass tubes (5 mm diameter, Norell inc., Landisville) in a glovebox, covered by a 4 mm glass block as spacer and subsequently sealed off tightly by using a fan burner immediately after locking them out of the box.

Low-temperature ^{2}H spectra between 38 K and room temperature were recorded using a single-resonance low-temperature probe (HPBB-LT ^{2}H, Bruker, Karlsruhe, $Q = 60$). The probe was placed in a cryostat STVP-200 (Janis Reasearch) which was cooled with liquid nitrogen or helium below ≈90 K. ^{2}H and ^{14}N spectra at moderate temperatures (160 K to room temperature) were recorded using a variable-temperature single resonance probe (HPBB-HT, Bruker, Karlsruhe, $Q = 90$ (^{2}H) or 45 (^{14}N)) with the heating being effected by a continuous stream of compressed air or dry nitrogen. The temperature stability was better than 0.5 K in the whole temperature range, and the temperature was accurate to about ±2 K. All probes were equipped with a solenoid coil with a diameter of 5 mm. The wide-line spectra were typically measured by applying a standard solid−echo impulse sequence[51] ($\pi/2_x - t_1 - \pi/2_y$ − acq) preceded by a saturation sequence. For suppression of the most frequent artifacts, the phase of the second pulse was cycled by $\phi \pm 90°$ with respect to the first, and both pulses were phase cycled by a cycle observation, yielding an eight-step phase cycle. Typical 90° pulse lengths were around 2.5 μs (^{2}H) or 2.0 μs (^{14}N), and the interpulse spacing was fixed to 20 μs for the low-temperature spectra and 40 μs for the high-temperature spectra (^{2}H) or 60 μs for ^{14}N. The dwell time was chosen between 0.1 and 2 μs (^{2}H) or 0.1 μs (^{14}N), attaching special attention to an accurate determination of the echo maximum. The recycle delay between the scans was adjusted to 3−5 times the relaxation time T_1 as determined by the saturation-recovery method.

For the kinetic studies, the sample was heated by a continuous flow of gaseous nitrogen in a sealed glass tube with a heating rate of 1 K min^{-1} to the respective target temperature between 372 and 380 K. Repeated acquisition at regular intervals was started at room temperature and spectra were typically recorded every 2.5−5 min during the first 3 h after reaching the target temperature, then increasing the repetition delay to 10 min, the temperature being stable within ±0.7 K. The scan recycle delay for the high-temperature spectra was fixed at 5 s, typically using a total of eight scans per spectrum.

Line-shape simulations were carried out with the program MXQET,[48] which allows to account for artifacts arising from finite pulse power and the dipolar interaction of the deuterons with their surroundings by convolution of the simulated spectra with a Gaussian function. Significant distortions of the experimental spectra arising from off-resonance effects and the asymmetries caused by the probe head were typically accounted for by introducing a linear attenuation spreading over the whole spectrum.

Since MXQET only provides an interface for simulations based on one single quadrupole-coupling constant, we designed a program for the simulation of ^{2}H line shapes associated with different QCC values based on the same mathematical procedure as described above, using the C++ library Gamma.[52] Some mathematical routines were carried out with the commercial program package MATLAB.[53]

Results and Discussion

Line-Shape Simulations. Wide-line ^{2}H NMR spectra of the ammonium ion in $ND_4[N(C{\equiv}N)_2]$ were recorded in a temperature range between 38 and 390 K; selected experimental spectra obtained by applying the solid−echo technique are displayed in Figure 2. Spectra recorded above room temperature will be discussed in a separate section.

On inspecting the line shapes, we can distinguish between four major dynamic regions: the high-temperature range (>230 K) is characterized by narrow (FWHM ≈ 6 kHz) spectra of non-Lorentzian type, whose line widths are slightly decreasing with increasing temperature. However, we do not observe completely motionally averaged spectra at room temperature typical of liquids which are composed of a single Lorentzian.

In the upper intermediate region ($160 < T < 190$ K) the spectral shape becomes increasingly featureless and collapses into a broadened quasi-Lorentzian line around 160 K. At even lower temperatures (100−150 K), a gradual crossover to a broad powder spectrum can be observed, the latter being characteristic of the slow-motion regime.

In the low-temperature range (<100 K), motion affecting the line shape is finally slowed down, leaving behind a superposition of three axially symmetric Pake spectra with slightly different QCCs and a common asymmetry parameter of essentially zero ($\eta = 0.02(1)$).

Finding an appropriate model of motion for the ammonium ion can be significantly facilitated by using the results of neutron diffraction as a starting basis:[21] Since in the whole temperature range the nuclear density of the deuterons is essentially

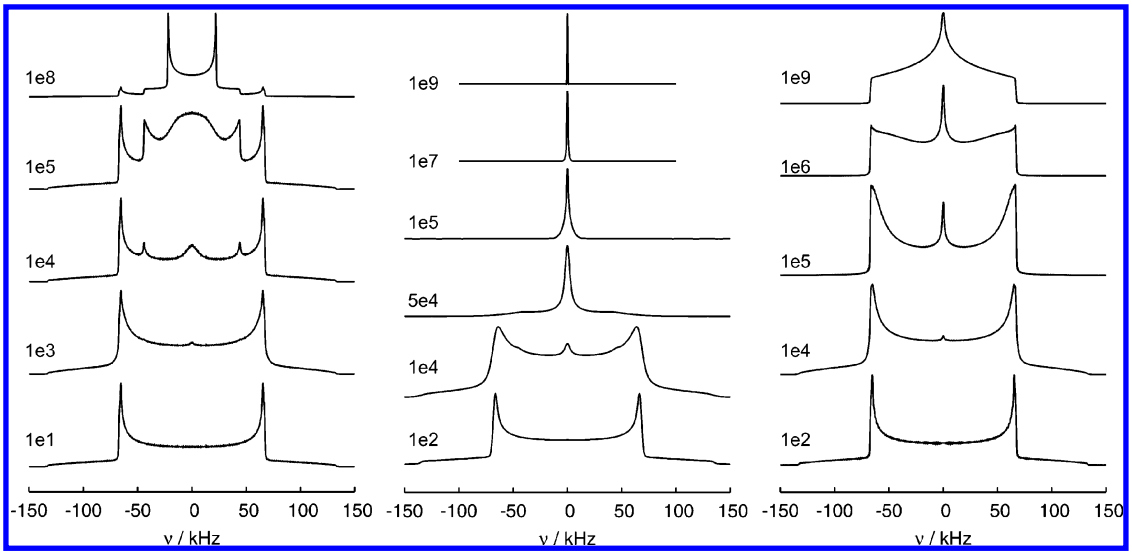

Figure 3. Line-shape simulations carried out for different jumping geometries: left, jumps about a single C_3 axis; middle, isotropic tetrahedral jumps; right, coupled 180° jumps of two pairs of deuterons about a single C_2 axis. Exchange frequencies are indicated in s^{-1}.

concentrated around the four tetrahedral sites, we can rule out models implying isotropic rotational diffusion of the ND_4^+ group in a flat potential with the deuteron sites distributed over spherical trajectories. Similarly, 90° jumps around the C_2 axes of the tetrahedron can be excluded, since this would increase the number of accessible deuteron sites to eight, which does not conform to the neutron diffraction data. Possible models are thus only those mapping all tetrahedral sites before and after the jump onto themselves. The latter scenario would be compatible with jumps of the tetrahedron about one of its 3-fold (C_3) or 2-fold (C_2) axes each, which are located along the N−D bonds or bisecting the D−N−D angles, respectively (cf. Figure 3 and the kinetic matrices given by eqs 5 and 4). These models should be observed preferentially if site symmetry constraints or characteristic distortions of the tetrahedral symmetry apply, the latter being for instance induced by the hydrogen-bonding network. The most intuitive model—if symmetry restrictions can be neglected as in the present case (ND_4^+ located on a general site with symmetry *1*)—is represented by a random four-site exchange of the deuterons, featuring an isotropic jump motion in a tetrahedral potential (eq 6). This model can be equally expressed as simultaneous jumps about all C_2 and C_3 axes and according line-shape simulations are depicted in Figure 3 (middle). For comparison, Figure 3 (left and right) displays simulations carried out for jumps in a strongly distorted 4-fold potential: 120° jumps around a single C_3 axis entail the superposition of a static spectrum (one static deuteron) with that of the three exchanging deuterons, which does not collapse into a single Lorentzian regardless of the exchange frequency (left). As outlined in Figure 3 (right), for simultaneous 180° jumps of two coupled pairs of deuterons separated by the tetrahedral angle about a single C_2 axis, one would expect a narrowing of the spectra, yet not a complete motional averaging in the high-frequency limit. As the line-shape simulations for a C_2 jump therefore differ significantly from those observed in the experimental spectra, this model of motion can be excluded as well.

From Figure 3 it gets evident that neither the two- nor the three-site exchange can satisfactorily reproduce the experimental spectra. According to the above line of argument, simulations based on a tetrahedral jump geometry were performed, including all-site exchange with equal a priori probabilities. Three noticeable aspects affecting the strategy of the simulations will be pointed out in the following:

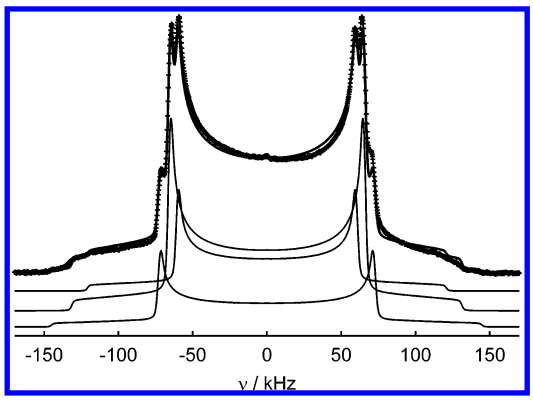

Figure 4. Deconvolution of a Pake spectrum of the ammonium group measured at 38 K. The spectrum (crosses) can be fitted (solid lines) by a superposition of three static spectra with different QCCs (161, 177, 193 kHz) and intensity ratios of 1:2:1.

TABLE 1: Fit Results for the Deconvolution of a Static ^{2}H Spectrum at 38 K

	(a)	(b)	(c)
QCC/kHz	193(2)	177(2)	161(2)
η	0.02(1)	0.02(1)	0.02(1)
intensity ratio	1	2.0(2)	1.1(2)

The first detail that has to be addressed is given by the existence of three quadrupole-coupling constants in the low-temperature spectra. According to line-shape simulations carried out with a program written to accommodate more than one QCC per ammonium group (cf. Experimental Methods), the spectra can be reproduced equally well by a simple superposition of three separate Pake spectra with QCCs between 161 and 193 kHz as demonstrated in Figure 4. Relevant fitting parameters are given in Table 1.

The intensity ratios obtained nicely sum up to a total of four Pake spectra corresponding to four N−D QCCs, two of which being essentially identical. Since only one crystallographically independent ammonium ion is present in the unit cell of $ND_4[N(C{\equiv}N)_2]$, the different Pake spectra can be associated with the four N−D bonds rather than with different types of ammonium ions. Since for a covalently bonded deuterium atom the electric field gradient is completely dominated by the electron distribution of the σ-bond and its orientation with respect to the external magnetic field, the magnitude of the

quadrupole-coupling constant is mainly determined by the strength of the N−D bond as well as dynamical processes affecting the interaction of the deuteron with the electric field gradient. Note that whereas at low temperatures the largest quadrupole-coupling constant of the spectra (193 kHz, cf. Table 1) corresponds to those expected for static N−D bonds of ammonium groups,[47,54,55] we simultaneously find smaller values (161 kHz) at low temperatures as well as a continuous decrease of the quadrupole-coupling constants from temperatures >133 K (125 kHz at 370 K). A possible explanation would be the presence of a process which leads to an effective reduction of the QCCs, even if the principal reorientational process is assumed to be unchanged. In agreement with the neutron diffraction data, librational motion of the deuterons on the surface of a cone can well account for the observed phenomenon. As ammonium ion librations are expected to be fast on the NMR time scale ($\tau^{-1} \gg$ 3/2 QCC), we will only refer to their influence on the spectra implicitly by starting from a reduced effective quadrupole-coupling tensor in the line-shape analyses. According to the spectral fits, the librational amplitudes change with temperature, and hence the resulting effective quadrupole-coupling tensor will also be a function of temperature (see below). Provided that the N−D bond strength is similar for all N−D bonds, a marked difference in the QCCs can only result from varying hydrogen-bonding strengths and, thus, degrees of librational motion of the four N−D bonds. Evaluation of the thermal displacement parameters of the deuterons by neutron diffraction suggests deuteron D2 to exhibit less pronounced thermal motion as compared to D1, D3, and D4 (for nomenclature, see Figure 1).[21,22] D2 could therefore be associated with the largest QCC, yet no satisfactory differentiation and, hence, assignment can be made for the remaining nuclei within experimental error.

Whereas in the slow motion region the spectra are reproduced well by the sum of three different subspectra, this is no longer valid in the high-temperature regime. Simulations performed with three effective QCCs systematically overestimate the width of the spectra above ≈160 K and do not account for the observed "shoulders" on both sides of the Lorentzian line (Figure 2). In general, one would expect the librational amplitudes of the deuterons to increase with temperature, thereby inducing a large-angle tumbling of the ND_4^+ group and a gradual loosening of the hydrogen-bonding network. As a consequence, the differences in the site frequencies are averaged out, and so are the quadrupole-coupling constants. Therefore, at temperatures above 160 K, a single QCC is sufficient for the simulation of the spectra.

As a second noticeable detail, the intensity in the center of the experimental spectra at intermediate temperatures (100−150 K) can only be satisfactorily accounted for by using a weighted superposition of a broad powder spectrum and a single Lorentzian line, although a sharp—yet weak—Lorentzian-type feature around the center frequency also arises from the simulations using a homogeneous jump process (Figure 3, middle, exchange frequency 1e4 s^{-1}). This observation also manifests itself in the biexponential behavior of the relaxation time between 120 and 160 K, the best fit being achieved by applying a double-exponential function accounting for two relaxational processes on a significantly different time scale and with differing weight (cf. section *Relaxation*). The T_1 for the second relaxation process was found to be around 10 ms, which is up to 4 orders of magnitude smaller than the one of the main relaxational process. Furthermore, it is essentially temperature independent in the small temperature window in which its spin−lattice relaxation time could be extracted. The noticeable increase of the intensity of the Lorentzian between 120 and 160 K can be attributed to the strong attenuation of the major part of the spectrum owing to the influence of the reduction factor caused by the solid−echo sequence, thereby distorting the true relative intensities. As the contribution of the second relaxational process is below 5% (estimated from the ^{2}H spectrum at 120 K) and does not influence the jump process of the ammonium ions in the bulk, a separate treatment of the two different relaxational processes seems to be justified. As possible sources for the observed Lorentzian, surface-adsorbed ammonium groups, volatile ND_3, or D_2O with liquid-like dynamics may be considered. Alternatively, according to a "domain" concept put forward in the literature, the presence of a small fraction of "bulk" (instead of surface) ammonium groups with shallow rotational potentials may be inferred, located in the domain walls separating domains with ammonium ions having higher rotational potentials.[55]

Third, when considering only a single QCC at high temperatures as outlined above, the high-temperature region of the experimental spectra can only be fitted accurately by introducing a distortion of the tetrahedral jump geometry (cf. section Properties of Ammonium Dicyanamide).

Thus, simulations performed with the sites being located on an ideal tetrahedron are contrasted with those based on different distortions of the tetrahedral geometry in Figure 5 (for a definition of the tetrahedral angles referred to in the following, see inset of Figure 5). The latter vary either in the magnitude or in type of the distortion. We have exemplarily chosen a compressed tetrahedral geometry, which is in effect undistinguishable from an elongation of the tetrahedron in the simulations, as the line shape is only affected by the magnitudes of the angles. For an ideal tetrahedron with $\Delta\gamma = \Delta\epsilon = 0°$, one would expect a liquid-like Lorentzian at high temperatures (Figure 3), whose width is about one-quarter of the experimental line width; we can therefore discard ideal tetrahedral geometry for the ND_4^+ ion in the high-temperature region. The same applies for a symmetrically compressed (or stretched) tetrahedron, for which we would expect a slightly broadened line with a clear symmetric splitting at fast reorientational frequencies. This effect is so pronounced that even distortions of as little as $\Delta\gamma = \Delta\epsilon = 1°$ would clearly show up in the spectrum. Around 190 K, a symmetrically distorted tetrahedron matches the experimental data quite well; the same holds true for an asymmetrically stretched tetrahedron, which is shown for a less pronounced distortion of $\Delta\gamma = 3.5°$ and $\Delta\epsilon = 0.5°$ in Figure 5. The high-temperature spectra do, however, not satisfactorily reproduce the experimental results as the spectral width of the signal—though slightly broadened—is still too small. The best fit is achieved when considering a significantly asymmetric distortion of the tetrahedral jump geometry at higher temperatures, which amounts to about $\Delta\gamma = 6°$ and $\Delta\epsilon = 0.5°$. The broadening of the Lorentzian as well as the characteristic "humps" of the otherwise straight flanks are thus reproduced quite smoothly. At temperatures below ≈210 K, the simulated line shapes overestimate the size of the spectrum, which prompts us to postulate a decreasing distortion of the tetrahedron with decreasing temperature. As can be seen from Figure 5, the influence of the distortion diminishes at still lower temperatures (<150 K), where simulations for different degrees of tetrahedral compression essentially yield identical spectra.

From a crystallographic point of view we would expect a distortion to take place at lower temperatures when rotational motion gradually freezes out and the cation no longer experi-

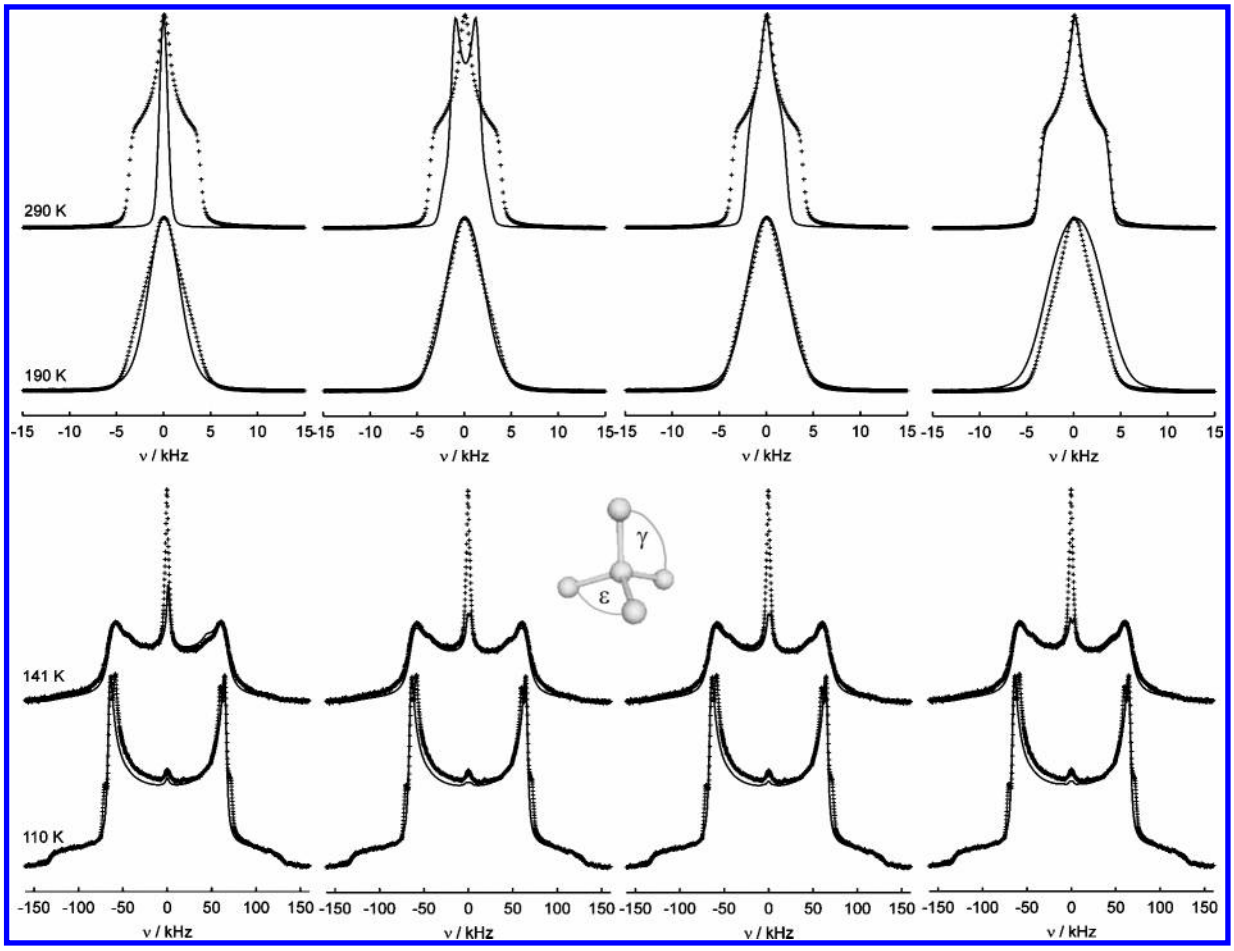

Figure 5. Experimental spectra (crosses) at 110−290 K (bottom to top) and simulations (solid lines) for different tetrahedral geometries with retention of at least one C_2 axis. Deviations $\Delta\gamma$ and $\Delta\epsilon$ from the tetrahedral angle are (from left to right): ideal tetrahedral symmetry, $\Delta\gamma = \Delta\epsilon = 0°$; symmetrically compressed (D_{2d} symmetry), $\Delta\gamma = \Delta\epsilon = 1°$; asymmetrically compressed (C_{2v} symmetry), $\Delta\gamma = 3.5°$; $\Delta\epsilon = 0.5°$; asymmetrically compressed, $\Delta\gamma = 6.0°$; $\Delta\epsilon = 0.5°$. The inset outlines the definition of the tetrahedral angles γ and ϵ used in the text.

ences an average crystal field. This effect could principally play a role in the case of ammonium dicyanamide as well, as we cannot distinguish between different degrees of distortions in the low-temperature region. It does, however, not seem straightforward to assume significant distortion in the low- *and* high-temperature region, with a temporal lifting of the distortion in the intermediate temperature range. This model is therefore not considered further.

A plausible source for the increasing distortion of the tetrahedron, however, is the anisotropic temperature dependence of the lattice parameters in ammonium dicyanamide.[21,22] The observed decrease of the *c*-axis comes along with a compression of the ammonium ion along an axis parallel to *c*, that is, roughly along the vector connecting D2 and D3 (cf. Figure 1). Therefore, the latter nuclei may approach each other with rising temperature, thus well giving rise to the observed distortion of one tetrahedral angle ($\Delta\gamma$) of ≈6°.

An independent proof of the tetrahedral distortion can be expected from ^{14}N ($I = 1$) NMR spectroscopy, as the quadrupolar broadening at the ammonium nitrogen would vanish in the case of perfect tetrahedral symmetry. Figure 6 displays two wide-line ^{14}N spectra obtained at different temperatures, exhibiting powder spectra with widths in the 0.8 MHz range. Owing to the limited spectral width of the probe and the final excitation width determined by the pulse length, it was not possible to accurately determine both the asymmetry and width of the spectra. Nevertheless, the obvious broadening of the spectra on going from low to high temperatures is interpreted in terms of a significant distortion of the tetrahedral symmetry. Following the above line of argument, however, an additional external electric field gradient at the low-symmetry site of the ammonium ion may also cause spectral broadening due to an increasing deviation of the local symmetry from ideally tetrahedral. However, as we cannot quantify this effect or its likely sources,

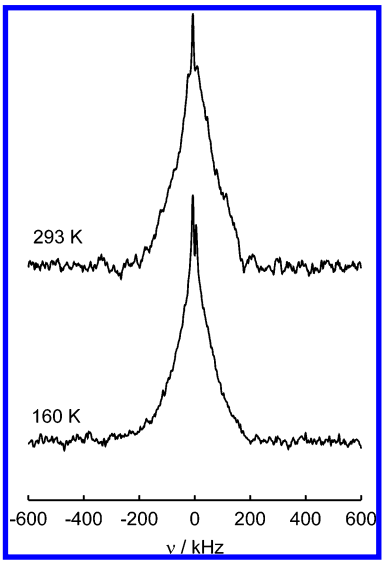

Figure 6. ^{14}N wide-line spectra measured at 160 K (bottom) and room temperature (top). The full width of the spectra (δ_{zz}) is disguised by technical problems associated with realizing larger excitation widths.

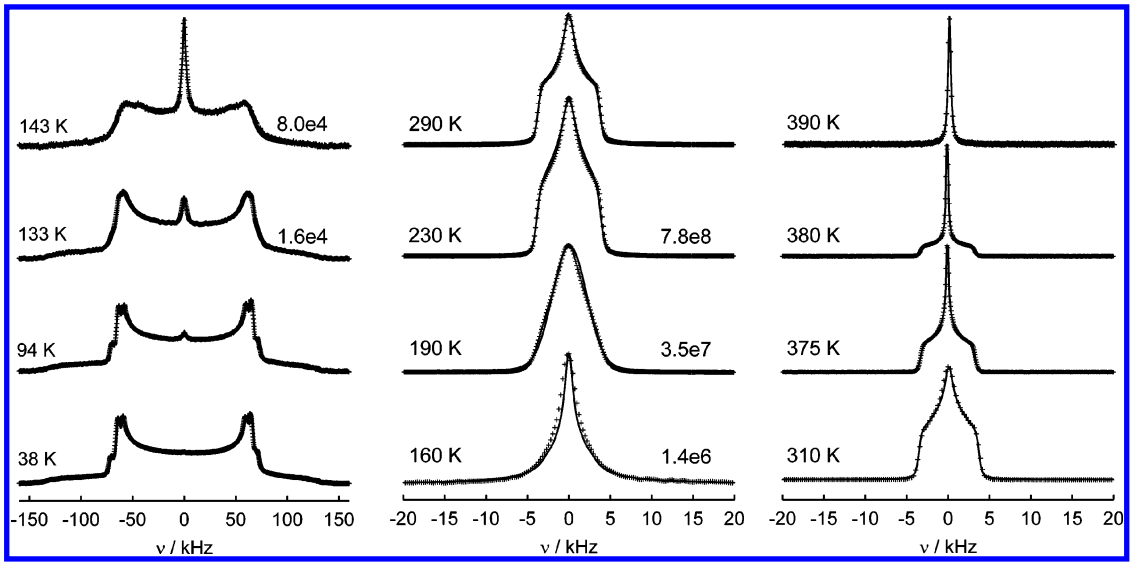

Figure 7. Experimental spectra obtained between 38 and 390 K, together with the respective line-shape simulations. Both a central Lorentzian and three QCCs at low temperatures (cf. text) were taken into account. Jump rates π_{ij} are given in s^{-1}. The high-temperature solid−echo spectra at $T \geq 375$ K already show signs of the transformation onset (increase of the central ND_3 signal).

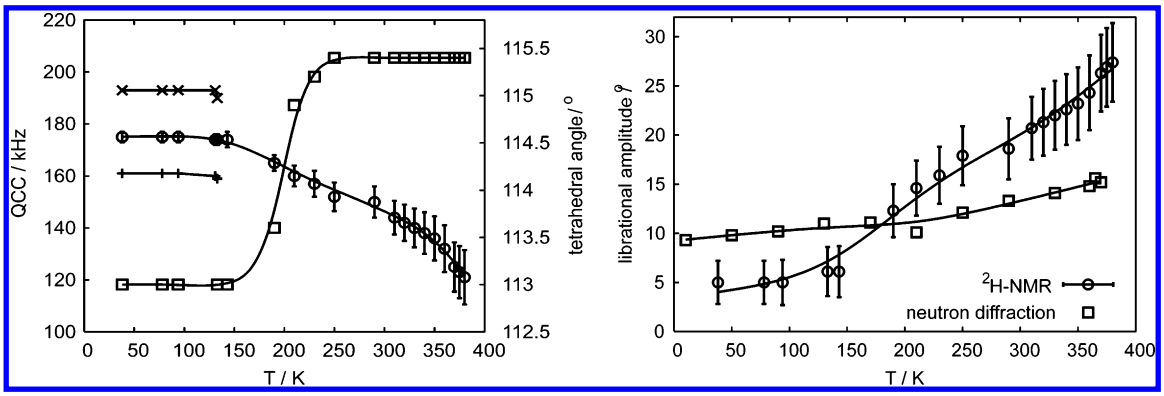

Figure 8. (left) Quadrupolar-coupling constants and tetrahedral distortion ($\Delta\gamma$, squares) as a function of temperature. (right) Librational amplitudes for the ammonium group obtained by wide-line ^{2}H NMR spectroscopy (circles) as a function of temperature, using a static QCC of 177 kHz and a simple cone-type librational model, and by rigid-body analysis of neutron powder diffraction data (squares).[21]

and a distortion of the ammonium group as outlined above also affords a nonvanishing quadrupole tensor, we consider the latter impact as the most likely source of spectral changes.

Using these findings as increments, based on which a general picture of the ammonium ion geometry and dynamics can be established, the results from the line-shape simulations between 38 and 390 K are outlined in Figure 7. In Figure 8, the change of the effective quadrupole-coupling constant is contrasted with the change of the tetrahedral distortion as obtained by the simulation as a function of temperature. In order to assess the librational amplitudes for the deuterons in the observed temperature range, we have used a common fixed QCC of 177 kHz at all temperatures as well as the respective reorientational frequencies obtained from the variable QCC-fits, leaving the librational amplitudes as the fitting parameter. Taking into account the neutron diffraction data,[21] we have to consider the presence of significant librational motion at the lowest temperatures accessible in the NMR experiment. When the static QCC is fixed at 177 kHz, the corresponding librational amplitude is 5° at 38 K, which seems a reasonable value at this temperature. The librational amplitudes calculated according to this procedure are displayed in Figure 8 (right), together with the amplitudes extracted by neutron diffraction for comparison. The librational amplitudes obtained from NMR were fitted by using an analytical function (solid line) based on a simple cone-type librational model with one-half of the cone opening angle being defined as the librational amplitude. We note that owing to the somewhat arbitrary choice of the starting parameters the values obtained from ^{2}H NMR should not be overinterpreted, the more so by considering the fact that the underlying models for librational motion are slightly different for the two experimental data sources, rendering a direct comparison critical. From inspection of both librational amplitudes and effective quadrupole-coupling constants (Figure 8), which are intrinsically linked with each other, we can associate the temperature range between 160 and 230 K with the most prominent dynamical changes. Most likely this feature correlates directly with the onset of ND_4^+ distortion developing with a sigmoidal increase as a function of temperature.

Relaxation. To increase the accessible frequency range of the relaxation rates and to test the homogeneity of the reorientational dynamics of the ammonium group beyond the fast motion limit, which is not accessible by line-shape analysis, the temperature dependence of the ^{2}H spin−lattice relaxation time was probed by applying a saturation-recovery sequence (Figure 9). The fast relaxational process attributed to a liquid-like reorientational behavior of a small fraction of ammonium groups (cf. above) was included into the refinement only between 120 and 160 K by using a double-exponential fit function; at all other temperatures, the relaxation behavior was found to be monoexponential. Accordingly, only the data for the dominating structural relaxation process were taken into

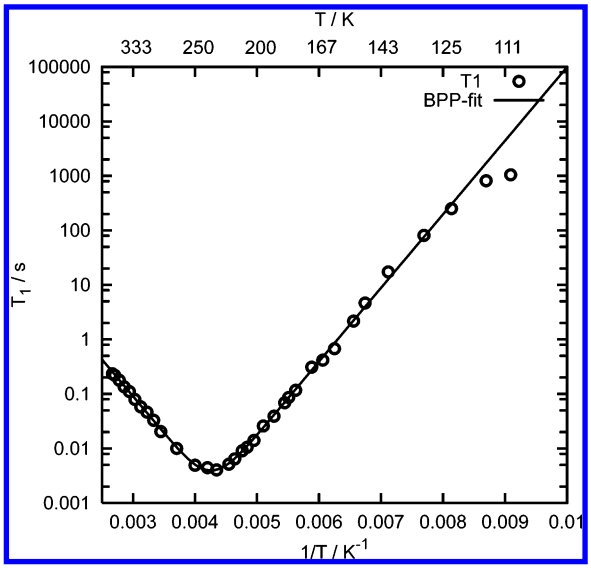

Figure 9. Spin−lattice (T_1) relaxation measurements for the reorientational motion of the ND_4^+ ion as a function of the inverse temperature. The experimental data (circles) are fitted by using a BPP-type model (solid line).

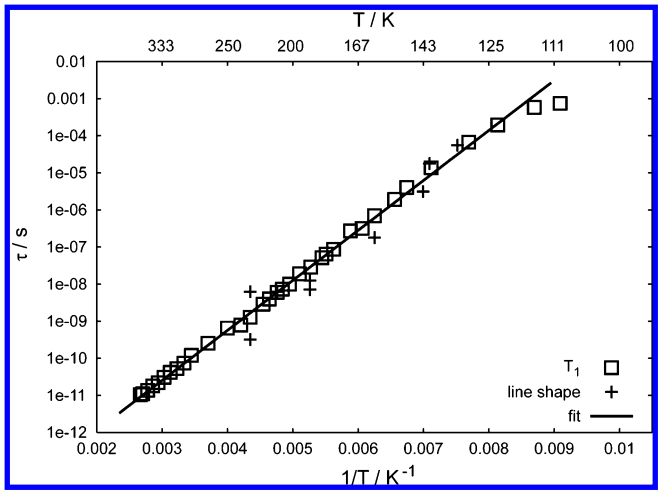

Figure 10. Arrhenius plot of the correlation time τ vs inverse temperature. Synopsis of the data obtained from T_1 relaxation measurements (squares) and those extracted from the line-shape analyses (crosses) by using the relation $\tau = (4\pi_{ij})^{-1}$. The spin−lattice relaxation data based on eqs 8 and 9 are considered more reliable owing to the larger number of data points and the smaller estimated standard deviation.

account for extracting the temperature dependence of the longitudinal relaxation time as given by Figure 9, the latter spanning a range between a minimum of 4 ms at 230 K to maximum values below 100 K of >2000 s. The data could be fitted by using a BPP equation (eq 8), corresponding well to an isotropic tetrahedral jump motion and an average QCC of the four deuterons of 177 kHz. By evaluating the spin−lattice relaxation rate T_1^{-1}, we can derive correlation times and jump rates for the reorientational processes (eqs 9 and 10). In Figure 10 the correlation times obtained from relaxation measurements as well as such obtained from line-shape analyses are plotted against the inverse temperature, yielding a linear dependence. From the Arrhenius-like temperature behavior and the magnitude of the attempt frequencies, we can classify the reorientational jumps as a thermally activated single-particle process. The slope of the straight line directly delivers the energy of activation for the jump process as 25.8(2) kJ mol^{-1} and an attempt frequency τ_0^{-1} of 440(80) THz. Compared to similar simple nondeuterated ammonium salts such as $(NH_4)_nX^{n+}$ (X = $SnCl_6$, BF_4, GeF_6, $PbCl_6$, ClO_4, $PtCl_6$, $PdCl_4$),[56−61] which exhibit activation energies in the order of 1.5−6.7 kJ mol^{-1}, this value appears to be at the upper end of the scale, which is indicative of comparatively high potential barriers for the reorientational motion of the ions due to rather strong hydrogen bonding of the ammonium group to the surrounding anions. This finding renders the presence of rotational diffusion highly unlikely as stated above: The latter type of motion comes along only with flat potential walls, typically occurring in the high-temperature region and displaying a nonclassical temperature behavior. A similarly high activation energy (25 kJ mol^{-1}) extracted from proton T_1 measurements has been reported for $NH_4[HF_2]$.[62] The magnitude of the jump rate τ^{-1} at the high-temperature end lies in the terahertz region and is therefore close to the frequencies of the lattice vibrations.

High-Temperature Studies. The conversion of ND_4*dca* into dicyandiamide has been investigated by in situ ^{2}H measurements between 370 and 390 K (Figures 7 (left) and 11). To record a close-to-real-time picture of the transformation process, we typically chose a slow heating rate (1 K min^{-1}), followed by isothermal treatment at the respective reaction temperature (372−380 K). The onset of the reaction was clearly indicated by the gradual growth of a central Lorentzian line with a width of roughly 500 Hz (FWHM). The increase of the Lorentzian was accompanied by a decrease of the ND_4^+ spectrum, which is shown at three different waiting times at 380 K in Figure 11 (left). An estimate of the relative fractions of the subspectra was carried out by deconvoluting the total spectrum and extracting the relative portions of the two contributing species as shown in Figure 11 (right). The Lorentzian can be attributed to highly mobile ND_3 being released during the reaction. Although theory and previous experiments already suggested ammonia to be a reactive intermediate during the transformation,[21,22] the evolution of the latter could be proven directly for the first time by the in situ ^{2}H NMR data. However, it cannot be decided on the basis of the 1D spectra alone whether the Lorentzian line originates from free ND_3 in the gas phase above the solid sample or is rather due to ND_3 adsorbed on the sample surface, or even "quasi-free" ND_3 diffusing through the bulk sample in statu nascendi. Toward the final phase of the reaction, spectra were recorded using longer recycle delays (200 s) so as to probe spectral fractions pertaining to slowly relaxing species, which were previously suppressed by applying short scan delays. By doing so, a broad Pake spectrum superposed on the narrow ammonia signal could be visualized, which most likely can be attributed to the product species dicyandiamide (Figure 12). Apart from small angle librations, the amino groups of the latter are expected to be largely static at the temperature under consideration, thus giving rise to a quasi-static powder spectrum as was observed in the experiment. The reduction of the ND_4^+ portion of the spectra proceeds on different time scales depending on the chosen target temperature. Interestingly, the evolution of ammonia does not—as could be expected—approach a limit value which is then maintained, since the reaction proceeds in a closed system. Contrarily, a gradual decrease of ammonia is observed beyond a certain point, which points to the successive "consumption" of ammonia as the reaction proceeds. The ammonia intensity is plotted in Figure 13 as a function of time at four different target temperatures between 372 and 380 K. The origin of the time axis is associated with the onset of heating at room temperature, which results in the release of ammonia being observed only shortly before reaching the target temperature after 80 min on average.

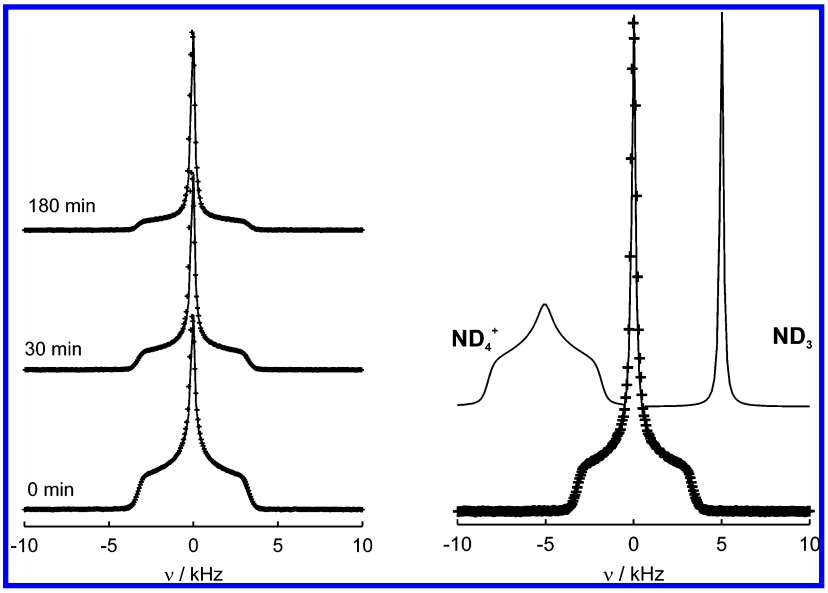

Figure 11. (left) Fits (solid lines) of the experimental spectra (crosses) recorded at 380 K for different tempering times. (right) The fit can be represented by the sum of two subspectra pertaining to ND_4^+ (broad spectrum) and ND_3 (Lorentzian).

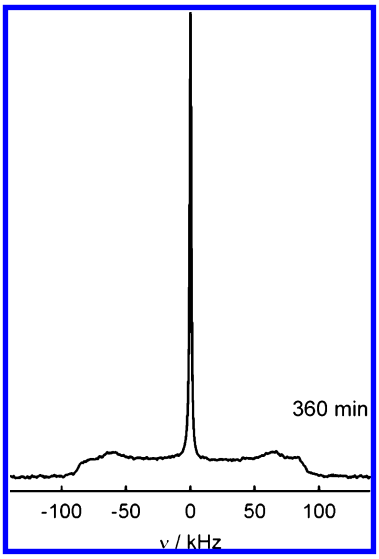

Figure 12. ^{2}H wide-line spectrum measured after a tempering time of 360 min at 380 K (recycle delay 300 s). The experimental spectrum is a superposition of a broad Pake spectrum, presumably originating from dicyandiamide, and the ND_3 Lorentzian.

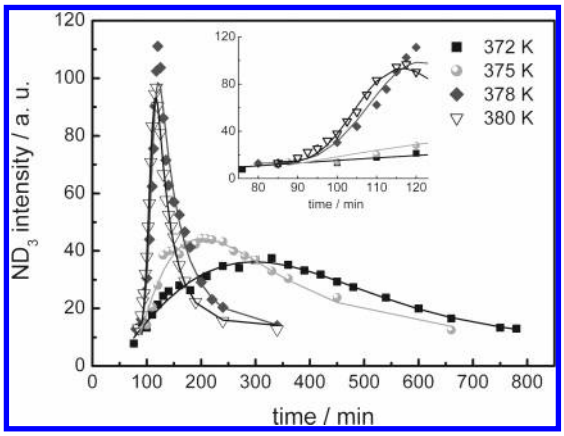

Figure 13. Time evolution of the scaled intensity of ND_3, monitored at 372 K (squares), 375 K (circles), 378 K (rhombuses), and 380 K (triangles) and fitted using a double exponential (eq 11). The growth of ammonia intensity is visualized enlarged in the inset.

The onset and initial velocity of ammonia evolution does not vary significantly with the target temperature chosen. For the lowest temperatures (372 and 375 K), however, the rate of ammonia evaporation decelerates steadily (negative curvature), whereas at 378 and 380 K a short "induction" phase is observed, followed by an acceleration period (positive curvature) and a terminal slowing down near the maximum ND_3 intensity. As a consequence, the maximum ND_3 intensity is reached significantly later at lower temperatures as compared to the situation at 378 and 380 K.

Since the generated ammonia is subsequently consumed stoichiometrically as the reaction toward dicyandiamide proceeds, we deal with two independent processes characterized by differing time constants, where the formation of ammonia is typically faster than its reassembly. The latter is much more attenuated at lower temperatures, proceeding on a time scale of several hours. At 372 K the decrease in ND_3 intensity apparently levels off after isothermal tempering for 12 h, suggesting the transformation did not proceed quantitatively within the experimental time window.

To parametrize the time evolution of the ammonia intensity, an Avrami-type equation was modified with an exponential decay as a function of the "reaction time" *t*. In its original form, the Avrami−Erofeev expression was developed for nucleation and crystal growth kinetics;[63−66] in the present context, however, it is simply used to continuously fit the observed change from both sigmoidal and decelerating growth to exponential decay. The isothermal yield−time curves are represented by

$$I(t) = I(0) + M_0 \exp[-((t - t_0)/\tau_1)^a]\{1 - \exp[-((t - t_0)/\tau_2)^b]\} \quad (11)$$

where M_0 is the fitting parameter for the maximum signal intensity. The most relevant fit parameters ($t_0 \approx 76 - 85$ min) are listed in Table 2. τ_2 accounts for the rate of ammonia evolution, while τ_1 is associated with the decrease of ND_3. By introduction of the exponents *a* and *b*, the curvature of both decay and slope can be suitably adjusted. From Table 2 it can be seen that τ_1 is similar for 378 and 380 K, whereas it is about 10 times larger at 375 K and almost 20 times at 372 K. Similar relations hold for τ_2, suggesting the rate of ND_3 evolution and

TABLE 2: Fit Results for the Time Dependence of Ammonia Evolution at 372, 375, 378, and 380 K, Using Equation 11[a]

parameter	372 K	375 K	378 K	380 K
τ_1	370(9)	180(11)	19(2)	16(2)
τ_2	345(23)	120(10)	36(2)	26(2)
a	1.8(3)	1.4(3)	0.7(1)	0.8(2)
b	1.0(2)	1.2(2)	4.2(6)	3.6(6)
I(0)	10(1)	11(2)	13(2)	14(2)

[a] The time constants τ_1 and τ_2 are given in minutes and the initial ND_3 intensity at the target temperature *I*(0) in arbitrary units.

consumption to increase significantly with isothermal temperature. Nevertheless, for temperatures ≥378 K the kinetics of both ND_3 evolution as well as decrease are similar and can hardly be distinguished within experimental error. *I*(0) accounts for the fact that no abrupt onset, but rather a smooth increase of ammonia evolution during the heating period, i.e., already before reaching the target temperature, is observed.

As outlined above, for the two lower temperatures a deceleratory kinetics, which can be translated into a consistent reduction of the rate of ammonia evolution, is observed, while a sigmoid-type curve best describes the growth kinetics for $T \geq 378$ K, corresponding to a change[67,68] of *b* from ≈1 at lower temperatures (first-order kinetics) to $b > 1$ at 378 and 380 K. In the latter temperature regime, a short "induction" time prior to the acceleratory growth is observed, which may be associated with a structural rearrangement (generation of defects, amorphization or microscopic melting) required for the release of ammonia from the former ammonium sites. After an acceleratory regime is passed at $T \geq 378$ K, the evolution of ammonia finally slows down at all temperatures, possibly induced by the ND_3 equilibrium pressure reached in the gas phase, which counteracts further evaporation of ammonia. Ammonia "reconsumption" can roughly be described using a Gaussian-type decay ($b \approx 2$) at lower temperatures, whereas at higher temperatures it becomes increasingly first order ($b \approx 1$), indicating the concentration of ammonia to be the rate-determining factor for the conversion of the presumed intermediate "$HN(CN)_2$" into dicyandiamide.

Considering the entire reaction process including the initial deuteron (proton) transfer, we are now able to draw a realistic picture of the different time scales on which the transformation proceeds: According to Schotte et al.,[69,70] a coupling between the relaxational single particle motion and lattice modes is possible if both are of the same order of magnitude. We can therefore argue that in the presence of fast reorientational motion of the ND_4^+ tetrahedra, the transfer of a deuteron to an adjacent anion is stimulated by the coupling of the jump motion to the lattice modes, thereby providing a mechanism for the deuteron detachment and the following transformation of the ionic ammonium dicyanamide into the molecular compound dicyandiamide. As the jumps of the ND_4^+ group can be considered to be instantaneous (cf. above), the dwell time of the deuterons (protons) on their actual sites roughly corresponds to the correlation time at temperatures above 370 K. Thus, the detachment of the deuteron (proton) is likely to proceed in a cooperative fashion upon translational−rotational coupling on a time scale in the order of 10^{-11} s. As the deuteron (proton) transfer is very fast, the rate-determining step of the overall reaction is not associated with the deuteron (proton) transfer but with the separation of ammonia from the ammonium sites, its diffusion through the sample, and its subsequent nucleophilic addition to the nitrile carbon. These processes may be retarded by a temperature gradient, giving rise to a nonuniform propagation of the transformation within the powdered sample. At any rate, the velocity of the *overall* transformation is in the order of minutes, which corresponds to a time regime typically encountered in solid-state reactions.

It has previously been observed that conducting the reaction under the pressure of ammonia facilitates the product formation and leads to significantly higher yields.[21,22] From the ^2H NMR experiments we can therefore add evidence that counterpressure of ammonia is essential for its re-uptake into the sample and stoichiometric consumption, which cannot be ensured if (a) ammonia is allowed to evaporate from the sample and (b) the reaction time is chosen too short with respect to the reaction temperature.

We note that prior to these investigations it has not been clear that reaction times beyond a minimum of 4 h have to be chosen in order to furnish satisfactory conversion and yield. If the reaction is terminated too early, a lack of ammonia will inevitably result in the formation of a large fraction of amorphous material, presumably the polymerization product of the free acid dicyanamide $HN(CN)_2$, which is formed together with ammonia in the first step of the reaction. Dicyanamide has long been known to be particularly acidic and, at the same time, highly susceptible to polymerization.[19,71] The question to which extent ammonia is inevitably "lost" in a side reaction, accompanied by polymerization of dicyanamide, cannot be decided unambiguously. To resolve this issue, a simultaneous in situ screening of the ^2H spectra of the starting material and the product would be necessary, which is critical owing to the long ^2H relaxation time in dicyandiamide.

Conclusions

^2H wide-line NMR was used to probe the ammonium ion dynamics of ND_4dca, with respect to both its reorientational behavior and its impact on the solid-state transformation of ammonium dicyanamide into dicyandiamide. Rapid isotropic reorientation of the ammonium group in a distorted tetrahedral potential is observed, which is associated with an activation energy and attempt frequency of roughly 25.8(2) kJ mol^{-1} and 440(80) THz, respectively. Simulations suggest that the ammonium group is distorted asymmetrically with a deviation from the tetrahedral angle of $\Delta\gamma \approx 6°$, $\Delta\epsilon \approx 0.5°$, with the extent of deformation increasing with increasing temperature. We could demonstrate that due to the reorientation rates being in the terahertz range at temperatures near the transformation onset, the latter may be stimulated by a coupling of the reorientational motion of the ammonium ion to the lattice modes. This "trigger" may initiate the proton transfer from the cation to the anion, which could be visualized indirectly by detecting the ammonia evolved during the reaction. Evidence was put forward that the isomerization reaction proceeds in a multistep fashion with the first step (proton transfer) being comparatively fast as compared to the nucleophilic addition of ammonia to the presumed intermediate dicyanamide. The reaction may be classified as a solid-state reaction proceeding with participation of the gas phase and, thus, as a heterogeneous solid−gas reaction. As a consequence, the yields of the transformation can greatly be enhanced by conducting the reaction under the pressure of ammonia and allowing for long reaction times.

Acknowledgment. We gratefully acknowledge financial support that was granted from the Deutsche Forschungsgemeinschaft DFG, Fonds der Chemischen Industrie FCI, the BMBF, and the Studienstiftung des Deutschen Volkes (scholarships for B. V. Lotsch).

References and Notes

(1) Cohen, M. L. *Phys. Rev.* **1985**, *B32*, 7988.
(2) Liu, A. Y.; Cohen, M. L. *Science* **1989**, *245*, 841.
(3) Niu, C.; Lu, Y. Z.; Lieber, C. M. *Science* **1993**, *261*, 334.
(4) Teter, D. M.; Hemley, R. J. *Science* **1996**, *271*, 53.
(5) Kroke, E.; Schwarz, M. *Coord. Chem. Rev.* **2004**, *248*, 493.
(6) Matsumoto, S.; Xie, E. Q.; Izumi, F. *Diamond Relat. Mater.* **1999**, *8*, 1175.
(7) Muhl, S.; Mendez, J. M. *Diamond Relat. Mater.* **1999**, *8*, 1809.
(8) Mattesini, M.; Matar, S. F.; Snis, A.; Etourneau, J.; Mavromaras, A. *J. Mater. Chem.* **1999**, *9*, 3151.
(9) Komatsu, T.; Nakamura, T. *J. Mater. Chem.* **2001**, *11*, 474.
(10) Komatsu, T. *J. Mater. Chem.* **2001**, *11*, 799.
(11) Komatsu, T. *J. Mater. Chem.* **2001**, *11*, 802.
(12) Alves, I.; Demazeau, G.; Tanguy, B.; Weill, F. *Solid State Commun.* **1999**, *109*, 697.
(13) Kouvetakis, J.; Bandari, A.; Todd, M.; Wilkens, B.; Cave, N. *Chem. Mater.* **1994**, *6*, 811.
(14) Jürgens, B.; Irran, E.; Senker, J.; Kroll, P.; Müller, H.; Schnick, W. *J. Am. Chem. Soc.* **2003**, *125*, 10288.
(15) Lotsch, B. V.; Döblinger, M.; Sehnert, J.; Seyfarth, L.; Senker, J.; Oeckler, O.; Schnick, W. *Chem. Eur. J.* **2007**, *13*, 4969.
(16) Wöhler, F. *Ann. Phys. (Berlin*) **1828**, *12*, 253.
(17) Liebig, J.; Wöhler, F. *Ann. Phys. Leipzig, Ser. 2* **1830**, *20*, 369.
(18) Dunitz, J.; Harris, K. D. M.; Johnston, R. L.; Kariuki, B. M; MacLean, E. J; Psallidas, K.; Schweizer, W. B.; Tykwinski, R. R. *J. Am. Chem. Soc.* **1998**, *120*, 13274.
(19) Madelung, W.; Kern, E. *Liebigs Ann. Chem.* **1922**, *427*, 1.
(20) Jürgens, B.; Höppe, H. A.; Irran, E.; Schnick, W. *Inorg. Chem.* **2002**, *41*, 4849.
(21) Lotsch, B. V.; Senker, J.; Kockelmann, W.; Schnick, W. *J. Solid State Chem.* **2003**, *176*, 180.
(22) Lotsch, B. V.; Senker, J.; Schnick, W. *Inorg. Chem.* **2004**, *43*, 895.
(23) Senker, J.; Müller, M.; Press, W.; Mayer, H. M.; Ibberson, R. M.; Jacobs, H. *Physica B* **1997**, *234*−*236*, 51.
(24) Müller, M.; Asmussen, B.; Press, W.; Senker, J.; Jacobs, H.; Büttner, H.; Kockelmann, W.; Ibberson R. M. Physi*ca B* **1997**, *234*−*236*, 45.
(25) Spiess, H. W.; Sillescu, H. *J. Magn. Res.* **1981**, *42*, 381.
(26) Böhmer, R.; Diezemann, G.; Hinze, G.; Rössler, E. *Prog. Nucl. Magn. Reson. Spectrosc.* **2001**, *39*, 191.
(27) Senker, J. Ph.D. thesis, University of Dortmund, 1996.
(28) Haarmann, F. Ph.D. thesis, University of Dortmund, 2001.
(29) Schmidt-Rohr, K.; Spiess, H. W. *Multidimensional Solid-State NMR and Polymers*; Academic Press: New York, 1994.
(30) Lusceac, S. A.; Roggatz, I.; Medick, P.; Gmeiner, J.; Rössler, E. A. *J. Chem. Phys.* **2004**, *121*, 4770.
(31) Lusceac, S. A.; Koplin, C.; Medick, P.; Vogel, M.; Brodie-Lindner, N.; LeQuellec, C.; Alba-Simionesco, C.; Rössler, E. A. *J. Phys. Chem.* **2004**, *43*, 16602.
(32) Blochowicz, T.; Karle, C.; Kudlik, A.; Medick, P.; Roggatz, I.; Vogel, M.; Tschirwitz, Ch; Wolber, J.; Senker, J.; Rössler, E. *J. Phys. Chem. B* **1999**, *103*, 4032.
(33) Senker, J.; Rössler, E. *J. Phys. Chem. B* **2002**, *106*, 7592.
(34) Vogel, M.; Rössler, E. *J. Chem. Phys.* **2001**, *114*, 5802.
(35) Vogel, M.; Rössler, E. *J. Chem. Phys.* **2001**, *115*, 10883.
(36) Schmidt, T.; Schmitt, H.; Haeberlen, U.; Olejniczak, Z.; Lalowicz, Z. T. *J. Chem. Phys.* **2002**, *117*, 9818.
(37) Birczynski, A.; Lalowicz, Z. T.; Łodziana, Z. *Chem. Phys.* **2004**, *299*, 113.
(38) Birczynski, A.; Lalowicz, Z. T.; Punkkinen, M.; Szymocha, A. M. *Chem. Phys.* **2006**, *327*, 373.
(39) Birczynski, A.; Lalowicz, Z. T.; Szymocha, A. M.; Punkkinen, M.; Ylinen, E. E.; Vuorimaki, A. H. *Chem. Phys.* **2006**, *327*, 119.
(40) Chiba, T. *J. Chem. Phys.* **1962**, *36*, 1122.
(41) Petch, H. E.; Cranna, N. G.; Volkoff, G. M. *Can. J. Phys.* **1963**, *31*, 837.
(42) Rabideau, S. W.; Waldstein, P. *J. Chem. Phys.* **1965**, *42*, 3822.
(43) Hovi, V.; Pyykkö, P. *Phys. Kondens. Mater.* **1966**, *5*, 1.
(44) Senker, *J. Solid State Nucl. Magn. Res.* **2004**, 26, 22.
(45) Wittebort, R. J.; Szabo, A. *J. Chem. Phys.* **1978**, *69*, 1722.
(46) Torchia, D. A.; Szabo, A. *J. Magn. Res.* **1981**, *49*, 107.
(47) Abragam, A. *Principles of Nuclear Magnetism*; Oxford Science Publications: Oxford, 1961.
(48) Greenfield, M. S.; Ronemus, A. D.; Vold, R. L.; Vold, R. R.; Ellis, P. D.; Raidy, T. E. *J. Magn. Res.* **1987**, *72*, 89.
(49) Senker, J.; Jacobs, H.; Müller, M.; Press, W.; Neue, G. *J. Phys. Chem. B* **1999**, *103*, 4497.
(50) Spiess, H. W. Rotation of Molecules and Nuclear Spin Relaxation; *NMR: Basic Principles and Progress*; Springer-Verlag: Berlin, 1978; Vol. 15.
(51) Davis, J. H.; Jeffrey, K. R.; Bloom, M.; Valic, M. I. *Chem. Phys. Lett.* **1976**, *42*, 390.
(52) Smith, S. A.; Levante, T. O.; Meier, B. H.; Ernst, R. R. *J. Magn. Reson.* A **1994**, *106*, 75.
(53) MATLAB, *The language of technical computing*, MathWorks Inc., 24 Prime Park Way, Natick, MA 01760-1500, Copyright 1984−1998.
(54) Lalowicz, Z. T.; Punkkinen, M.; Olejniczak, Z.; Birczynnski, A.; Haeberlen, U. *Solid State Nucl. Magn. Res.* **2002**, *22*, 373.
(55) Filipek, P.; Lalowicz, Z. T.; Olejniczak, Z.; Birczynnski, A. *Chem. Phys. Lett.* **2003**, *367*, 55.
(56) Prager, M.; Badurch, G. *J. Phys. C: Solid State Phys.* **1986**, *19*, 6105.
(57) Bonori, M.; Terenzi, M. *Chem. Phys. Lett.* **1974**, *27*, 281.
(58) Hennel, J. W.; Lalowicz, Z. T.; *Proc. XVI Congress Ampere*, Bucharest, Rumania 1971, p 637.
(59) Ylinen, E. E.; Tuohi, J. E.; Niemela, L. K. E. *Chem. Phys. Lett.* **1974**, *24*, 447.
(60) Riehl, J. W.; Wang, R.; Bernard, H. W. *J. Chem. Phys.* **1973**, *58*, 508.
(61) Güttler, W.; von Schültz, J. V. *Chem. Phys. Lett.* **1973**, *20*, 133.
(62) Reynhardt, E. C.; Watton, A.; Petch, H. E. *J. Chem. Phys.* **1979**, *71*, 4421.
(63) Avrami, M. *J. Chem. Phys.* **1939**, *7*, 1103.
(64) Avrami, M. *J. Chem. Phys.* **1940**, *8*, 212.
(65) Avrami, M. *J. Chem. Phys.* **1941**, *9*, 177.
(66) Li, Y. Q.; Zhang, L. *J. Phys.: Condens. Matter* **2003**, *15*, 8081.
(67) Avrami, M. *J. Chem. Phys.* **1940**, *8*, 212.
(68) Avrami, M. *J. Chem. Phys.* **1941**, *9*, 177.
(69) Schotte, U.; Schotte, K. D.; Kabs, M.; Dachs, H. *J. Phys.: Condens. Matter* **1992**, *4*, 9283.
(70) Schotte, U.; Schotte, K. D.; Bleif, H.-J.; Kabs, M.; Dachs, H. *J. Phys.: Condens. Matter* **1995**, *7*, 7453.
(71) Jürgens, B. Ph.D. thesis, University of Munich, Shaker Verlag: Aachen, 2004.